THE JOURNAL OF PHYSICAL CHEMISTRY C

Article

Cite This: J. Phys. Chem. C 2018, 122, 2041−2045

pubs.acs.org/JPCC

Cyclopropenium $(C_3H_3)^+$ as an Aromatic Alternative A-Site Cation for Hybrid Halide Perovskite Architectures

Thomas W. Kasel,[†] Alexander T. Murray,*[,‡] and Christopher H. Hendon*[,†]

[†]Materials Science Institute, Department of Chemistry and Biochemistry, University of Oregon, Eugene, Oregon 97403, United States

[‡]Department of Chemistry, Massachusetts Institute of Technology, Cambridge, Massachusetts 02139, United States

Supporting Information

ABSTRACT: Hybrid halide perovskites are an emerging class of photovoltaic materials, boasting high solar efficiencies from relatively simple preparations. However, the chemical diversity of the A-site organic cation is limited, generally due to steric constraints of the $(PbI_3)^-$ cage. Herein we describe the use of a non-benzenoid Hückel aromatic, $(C_3H_3)^+$, as a viable alternative to the readily employed methylammonium, formamidinium, and guanidinium A-site cations. $(C_3H_3)^+$ may lead to greater moisture stability due to the lack of an acidic proton relative to the current $(H{-}NR_3)^+$-based systems while still boasting a narrow electronic band gap (E_g = 1.5 eV) and mobile holes and electrons (m_h^* = −1.27 and m_e^* = 0.77, respectively).

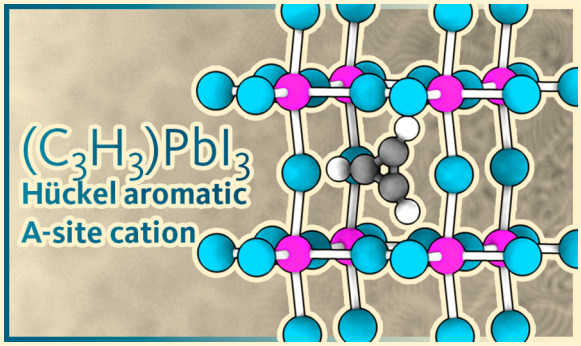

INTRODUCTION

The study of organic cations intercalated in metal halide anionic lattices has existed since Wyckoff's report in 1928,[1] but the recent explosion of interest stems from the seminal work of Kojima et al.[2] who demonstrated the use of a hybrid halide perovskite (of the form ABX_3, where methylammonium occupies the A-site) as a photoabsorber in a photovoltaic cell. Following this report, methylammonium lead iodide[3−9] and other hybrid halide perovskites have become a paradigm in solar energy production[10] and have sparked persistent interest because of their high light-to-electricity efficiency (advances from 9%[11] to a current record of 22.1%[12] in only 5 years) and ease and rapidity of synthesis.

Unlike the all-inorganic cesium analogue, $CsPbI_3$, the presence of the molecular dipole of methylammonium gives rise to a suite of unusual physical properties including ferroelectricity[13−16] and the occurrence of several crystallographically dissimilar phases.[17,18] While the physical properties of the material are clearly dependent on the nature of the monovalent cation, the electronic structure is less obviously so. In essentially all reported hybrid halide structures composed of Pb and I the frontier electronic bands have I-p and Pb-s,p character,[19] as well as similar band gaps to one another.[20] To further belabor this point, ammonium,[21] formamidinium,[22] acetamidinium,[23] and guanidinium[24] have been incorporated as alternative cations into similar systems, all of which share comparable electronic structure and physical properties to their methylammonium analogue.

While the compositional landscape is limited for both the B and X-site ions[25,26] (as determined by the redox potential of elements on the periodic table), the lack of diversity at the A-site is remarkable. Generally, the key advantages of using organic moieties in materials chemistry are the ability to electronically and sterically tune the compound of interest in a predictable and controlled manner. For example, in an attempt to increase the pK_a of the acidic methylammonium proton one may elect to use the formamidinium cation due to its delocalized positive charge. However, in the case of hybrid halide perovskites only a handful of organic A-site cations have been constructed, some shown schematically Figure 1.

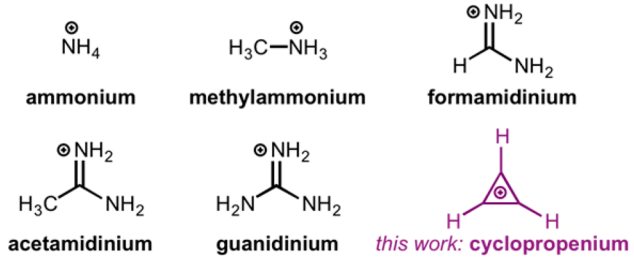

Figure 1. Some of the reported organic A-site cations found in $(PbI_3)^-$-based perovskites. The cyclopropenium cation differs from the other cations as it is aprotic.

The organic A-site cations depicted in Figure 1 share two things in common: they are small enough to fit inside the $(PbI_3)^-$ cage and they are singly charged. In the former, the size limitation is neatly summarized by comparison of the radius tolerance factors.[27,28] In the latter, there are only a limited number of ways to bestow a permanent positive charge on an

Received: December 1, 2017
Revised: January 4, 2018
Published: January 5, 2018

DOI: 10.1021/acs.jpcc.7b11867
J. Phys. Chem. C 2018, 122, 2041−2045

organic (i.e., H, C, N, O based) material, the most trivial being through protonation of a Lewis base lone pair. However, while acid/base chemistry is conceptually simple and allows rapid synthesis from common iodide salts the use of protic cations is detrimental for crystal stability (i.e., elimination of HI is thermodynamically favorable[29] and cation deprotonation or molecular disproportionation leads to gas formation and entropically motivated decomposition).[30,31] Therefore, the discovery of a novel organic cation that is both stable and small may mitigate some difficulties currently faced by $(CH_3NH_3)PbI_3$ and other protic hybrid halide perovskite architectures.

Here we describe an *aprotic, all-hydrocarbon* hybrid intercalator by drawing on non-benzenoid arene chemistry.[32] The $(C_3H_3)^+$ cation possesses Hückel aromaticity and has been isolated in both the hydrogenic and halogenated forms.[33−37] The parent $(C_3H_3)^+$ ion can be synthesized by Lewis acid mediated chloride elimination from C_3H_3Cl[38] or elimination of carbon monoxide and methanol by the action of Brønsted acid on cyclopropenyl ester $C_3H_3CO_2CH_3$.[39] While these carbocations are remarkably stable in solution phase, the stability should not grossly differ as their stability depends on their surrounding dielectric medium. Although we did not attempt a synthesis here, we do offer two potential synthetic routes, Scheme 1, that involve either the treatment of iodocyclopropene, C_3H_3I,[38,40] with PbI_2 or the decarbonylation of $C_3H_3CO_2CH_3$ with hydrogen iodide[39] in the presence PbI_2.

Scheme 1. Possible Synthetic Routes to $(C_3H_3)PbI_3$[a]

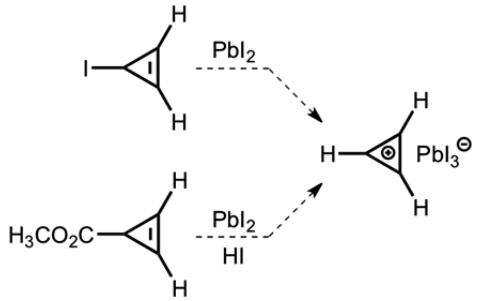

[a]The Lewis acid mediated iodide elimination is adapted from ref 38, while the decarbonylation is adapted from ref 39.

Despite its aromatic nature $(C_3H_3)^+$ has not been widely employed in functional materials; however, substituted derivatives have been used extensively for catalysis[41−43] and also as electrolyte components.[44] In this work we use density functional theory (DFT) calculations to demonstrate the electronic properties of the hypothetical target material $(C_3H_3)PbI_3$ with aim of motivating research into the application of $(C_3H_3)^+$ in hybrid halide perovskite architectures.

RESULTS AND DISCUSSION

First, we assessed the feasibility of $(C_3H_3)^+$ by examination of the revised tolerance factor.[28] Given $(C_3H_3)^+$ is only marginally larger than methylammonium, we estimate the tolerance factor to be 0.96, suggesting that its incorporation into the $(PbI_3)^-$ lattice is feasible. We constructed $(C_3H_3)PbI_3$ by making an A-site substitution to the low-temperature orthorhombic phase of $(CH_3NH_3)PbI_3$. Subsequent geometric and electronic optimization was performed using the procedure detailed in the Methods section. The resultant structure was found to be orthorhombic (lattice vectors: a = 6.305, b = 6.201, c = 6.374 Å).

The electronic band structure of $(C_3H_3)PbI_3$ shows the persistent characteristic features of most lead iodide based perovskites (Figure 2a). Notably, the incorporation of $(C_3H_3)^+$

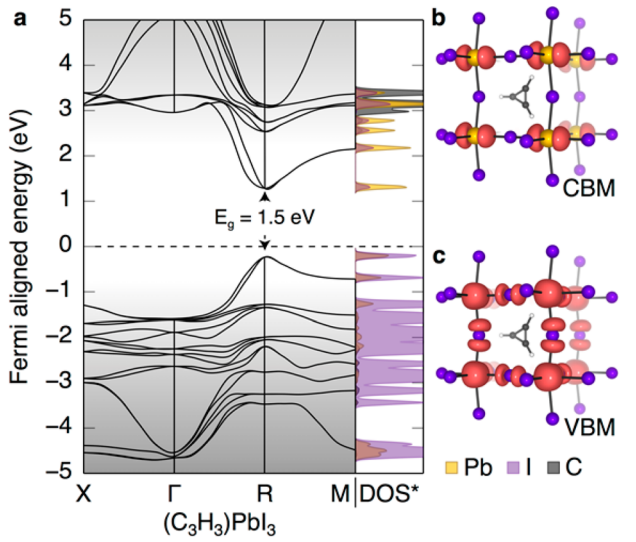

Figure 2. (a) Electronic band structure and density of states of $(C_3H_3)PbI_3$ as computed with HSE06sol+SOC (PBEsol with 43% HF exchange and spin−orbit coupling). (b and c) The conduction band minimum and valence band maximum orbital contributions at the R-point. Electron density isosurface is plotted in salmon at 0.006 e/Å^3. Density of states are plotted for special k-points, only*.

retains a direct electronic transition at the R-point and reasonable curvature at the valence band maximum (VBM) and conduction band minimum (CBM). Effective masses of holes and electrons were found to be m_h^* = −1.27 and m_e^* = 0.77, respectively.

Like other hybrid halide perovskites, the conduction band is composed of primarily Pb-p states (as evidenced by Figure 2b and the density of states). The VBM remains I-p and Pb-s centered, largely the same as $(CH_3NH_3)PbI_3$ (Figure 2c). Furthermore, while the band gap is highly dependent on the computational approach, the inclusion of $(C_3H_3)^+$ does not significantly alter the band gap compared to its methylammonium analogue, with $(C_3H_3)PbI_3$ featuring an electronic gap (E_g) = 1.5 eV (from HSE06sol+SOC with 43% HF exchange). PBEsol was also tested and produced E_g = 1.3 eV.

Considering the desirable electronic properties of $(C_3H_3)PbI_3$, we next assess the dynamic stability of the orthorhombic phase.

The role of hydrogen bonding in the methylammonium hybrid halide perovskite materials is still under investigation.[45−47] Given the nature of the N−H bond, hydrogen bonding will almost certainly affect the dynamics of any protic A-site cation, whose acidic proton is attracted to the bridging iodides. It should be noted, however, that intermolecular H-bonds could be beneficial in the formation of $(CH_3NH_3)PbI_3$ but would also give rise to strong acid−base interactions with water. While $(C_3H_3)^+$ would not be assumed to be a strong hydrogen-bond donor, we nevertheless explored this possibility. We note that the geometrically optimized structure produced from our DFT calculations yields two distinct C−C bond lengths in the $(C_3H_3)^+$ ring (1.365 and two 1.734 Å). The bond

DOI: 10.1021/acs.jpcc.7b11867
J. Phys. Chem. C 2018, 122, 2041−2045

length anisotropy is due to polarization installed by the $(PbI_3)^-$ cage deformation and the static nature of the DFT calculation. Using ab initio molecular dynamics simulations we are able to sample the A-site cation mobility (and therefore the A-site–cage interaction energy). We observe that $(C_3H_3)^+$ can translate along the plane in which it points; one such trajectory is presented in Figure 3a. This motion occurs along a shallow potential energy surface (Figure 3b) suggesting that the A-site cation is mobile. As expected, we did not observe orientation of the A-site C–H proton toward a bridging I^-, as the cyclopropenium is a poor hydrogen-bond donor.

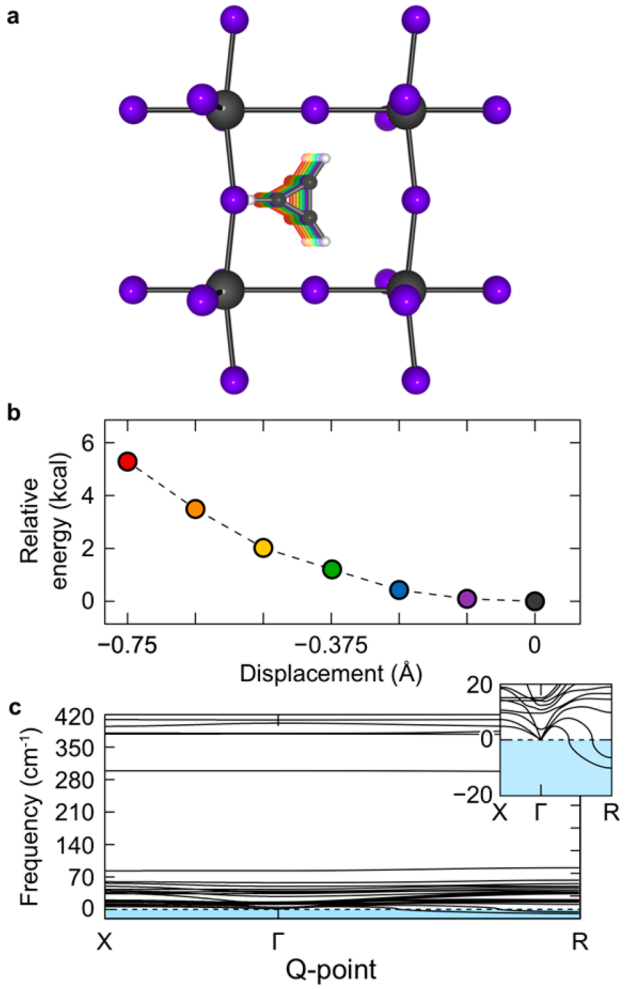

Figure 3. (a) Seven displacements of the A-site cation. The trajectory was obtained from an ab initio molecular dynamic simulation performed in triplicate. (b) Corresponding energies of displacement suggest that $(C_3H_3)^+$ ions are at least translation mobile at room temperature. (c) Examination of the phonon band structure shows no negative modes at Γ, and the usual negative modes—emphasized in the inset of panel c—associated with $(PbI_3)^-$ cage deformation when sampling in the *R*-vector, similar to that observed in $(CH_3NH_3)PbI_3$.

We compute the phonon band structure to assess the structural stability of our orthorhombic structure (Figure 3c). We note that there are no negative modes at the Γ-point and, like $(CH_3NH_3)PbI_3$, we see negative acoustic modes when sampling Γ-to-R, associated with $(PbI_3)^-$ cage deformation/structural transitions. Hence, we suspect that $(C_3H_3)PbI_3$ is, at minimum, metastable and likely exists in a similar chemical space to its other hybrid cousins.

Indeed, the orthorhombic phase is only one of several possible structural phases that $(C_3H_3)PbI_3$ may crystallize in. Short of an exhaustive structure search, we elected to include a second plausible hypothetical phase. Beginning with the α-phase[48] observed for $(CH(NH_2)_2)PbI_3$, cation substitutions were made and the structure was fully optimized; the resultant structure was triclinic (see the Supporting Information for the optimized structure of both phases). The significant increase in unit cell size prevents a full analysis of the phonon band structure, but we were able to assess dynamic stability through the omission of negative phonon modes at the Γ-point only. The electronic band gap was computed to be comparable to the orthorhombic phase, and the α-phase is predicted to lie on a relatively shallow potential energy surface and to be more stable by 5 kcal/mol. The α-phase is further dissimilar to the orthorhombic phase as the $(C_3H_3)^+$ ions are aligned in a diagonal fashion, rather than coplanar to a lattice plane (this is best visualized by examination of the optimized structures, presented in the Supporting Information).

CONCLUSIONS

In summary, the use of $(C_3H_3)^+$ in $(PbI_3)^-$ halide perovskite-type architectures provides interesting avenues and potential improvements in three key areas that trouble other hybrid alternatives. (1) The water instability of protic A-site cations may be remediated by the use of an *aprotic* cation such as the cationic annulene described in this paper. (2) $(C_3H_3)^+$ possesses no permanent dipole, thus obviating charging effects and other anomalous behavior observed in the literature. (3) The similar band gap compared to existing hybrid technologies should lead to comparable performance of the chromophore. Finally, we must comment on the reactivity and stability of $(C_3H_3)^+$. Indeed, there are new challenges associated with the cyclopropenium cation, and our current synthetic approach will likely have to be altered to realize this material. Furthermore, the more easily handled covalently halogenated cyclopropeniums are not feasible A-site cations in the 3D connected perovskites, due to the size requirements imposed by the $(PbI_3)^-$ cage but may offer interesting targets for 2D and layered architectures.

METHODS

Beginning with the experimentally determined crystal structure of the orthorhombic methylammonium lead iodide the A-site cation was substituted for C_3H_3. The material remained charge-neutral as the cyclopropenium caries a single positive charge in this framework. The structure was then geometrically and electronically optimized with the DFT construct as implemented in VASP. A 500 eV planewave cutoff, PBEsol, and a 6 × 6 × 6 *k*-grid was use to ensure electronic convergence to within 0.001 eV per atom, and the resultant structure was found to be orthorhombic. A similar procedure was employed for the modification of α-$(CH(NH_2)_2)PbI_3$. A 4 × 4 × 2 *k*-grid was used, and full optimization was performed. The resultant structure was triclinic. Tolerance factors were computed using r_{Pb} = 1.03, r_I = 2.20, and r_{C3H3} = 2.16 Å, yielding a tolerance factor of 0.96.

Typically, both Pb and I require spin–orbit coupling for accurate electron energies. However, the systematic underestimation of electronic band gap produced by PBEsol has been shown to recover the correct electronic band gap for these materials.[49] Here we use PBEsol as a first approximation and

DOI: 10.1021/acs.jpcc.7b11867
J. Phys. Chem. C 2018, 122, 2041–2045

compute the electronic band gap to be 1.3 eV. To recover a better electronic description of $(PbI_3)^-$ materials we employed the HSE06sol functional with an increased mixing of exact HF exchange (43%) and spin−orbit coupling. A similar procedure has been previously fruitful in predicting electronic properties of this class of materials.[26,50] In the text we refer to this method as HSE06sol+SOC, and it yielded E_g = 1.5 eV. The electronic band structure is computed using the geometric output from the PBEsol optimization with the HSE06sol+SOC used to sampling along the *k*-vectors (Figure 2). With exception to $(NH_4)PbI_3$, all hybrid halide perovskites are *P*1. Hence, we approximate the high symmetry point vectors and nomenclature using those assigned formally to the $CsPbI_3$ material, space group *Pm*-3*m*.

Effective masses were computed using the Effective Mass Calculator as presented by Fonari and Sutton,[51] accessed September 9, 2017. *K*-point sampling was made using a step size of 0.01 $bohr^{-1}$. The phonon band structure was computed using PhonoPy[52] by construction of a 2 × 2 × 2 supercell. Finite displacements were then used to compute the forces, using a tightened convergence criterion (0.0005 eV per atom).

Ab initio molecular dynamics was employed to investigate the dynamic stability of the $(C_3H_3)^+$ cation. A relaxed cutoff of 400 eV and Γ-only *k*-grid sampling was used. Simulations were run in triplicate to ensure no anomalous results, with a time step of 0.5 fs, heating at 0.1 K per geometric step from 0 to 500 K.

■ ASSOCIATED CONTENT

Supporting Information

The Supporting Information is available free of charge on the ACS Publications website at DOI: 10.1021/acs.jpcc.7b11867.

DFT-optimized structure of orthorhombic $(C_3H_3)PbI_3$ (CIF)

DFT-optimized structures of α-phase of $(C_3H_3)PbI_3$ (CIF)

■ AUTHOR INFORMATION

Corresponding Authors

*E-mail: murraya@mit.edu.

*E-mail: chendon@uoregon.edu.

ORCID

Thomas W. Kasel: 0000-0002-3695-8371

Alexander T. Murray: 0000-0002-7914-8205

Christopher H. Hendon: 0000-0002-7132-768X

Notes

The authors declare no competing financial interest.

■ ACKNOWLEDGMENTS

Computational work made use of the Extreme Science and Engineering Discovery Environment (XSEDE), which is supported by the National Science Foundation Grant No. ACI-1053575. This work benefited from access to the University of Oregon high performance computing facility (UO-TALAPAS).

■ REFERENCES

(1) Wyckoff, R. W. G. The Crystal Structures of Monomethyl Ammonium Chlorostannater and Chloroplatinate. *Am. J. Sci.* **1928**, *s5-16*, 349−359.

(2) Kojima, A.; Teshima, K.; Shirai, Y.; Miyasaka, T. Organometal Halide Perovskites as Visible-Light Sensitizers for Photovoltaic Cells. *J. Am. Chem. Soc.* **2009**, *131*, 6050−6051.

(3) Snaith, H. J. Perovskites: The Emergence of a New Era for Low-Cost, High-Efficiency Solar Cells. *J. Phys. Chem. Lett.* **2013**, *4*, 3623−3630.

(4) de Quilettes, D. W.; Vorpahl, S. M.; Stranks, S. D.; Nagaoka, H.; Eperon, G. E.; Ziffer, M. E.; Snaith, H. J.; Ginger, D. S. Impact of Microstructure on Local Carrier Lifetime in Perovskite Solar Cells. *Science* **2015**, *348*, 683−686.

(5) Green, M. A.; Ho-Baillie, A.; Snaith, H. J. The Emergence of Perovskite Solar Cells. *Nat. Photonics* **2014**, *8*, 506−514.

(6) Boix, P. P.; Agarwala, S.; Koh, T. M.; Mathews, N.; Mhaisalkar, S. G. Perovskite Solar Cells: Beyond Methylammonium Lead Iodide. *J. Phys. Chem. Lett.* **2015**, *6*, 898−907.

(7) Christians, J. A.; Manser, J. S.; Kamat, P. V. Best Practices in Perovskite Solar Cell Efficiency Measurements. Avoiding the Error of Making Bad Cells Look Good. *J. Phys. Chem. Lett.* **2015**, *6*, 852−857.

(8) Shi, D.; Adinolfi, V.; Comin, R.; Yuan, M.; Alarousu, E.; Buin, A.; Chen, Y.; Hoogland, S.; Rothenberger, A.; Katsiev, K.; et al. Low Trap-State Density and Long Carrier Diffusion in Organolead Trihalide Perovskite Single Crystals. *Science* **2015**, *347*, 519−522.

(9) Huang, J.; Yuan, Y.; Shao, Y.; Yan, Y. Understanding the Physical Properties of Hybrid Perovskites for Photovoltaic Applications. *Nat. Rev. Mater.* **2017**, *2*, 17042.

(10) Lee, M. M.; Teuscher, J.; Miyasaka, T.; Murakami, T. N.; Snaith, H. J. Efficient Hybrid Solar Cells Based on Meso-Superstructured Organometal Halide Perovskites. *Science* **2012**, *338*, 643−647.

(11) Kim, H.-S.; Lee, C.-R.; Im, J.-H.; Lee, K.-B.; Moehl, T.; Marchioro, A.; Moon, S.-J.; Humphry-Baker, R.; Yum, J.-H.; Moser, J. E.; et al. Lead Iodide Perovskite Sensitized All-Solid-State Submicron Thin Film Mesoscopic Solar Cell with Efficiency Exceeding 9%. *Sci. Rep.* **2012**, *2*, 591.

(12) Yang, W. S.; Park, B.-W.; Jung, E. H.; Jeon, N. J.; Kim, Y. C.; Lee, D. U.; Shin, S. S.; Seo, J.; Kim, E. K.; Noh, J. H.; et al. Iodide Management in Formamidinium-Lead-Halide−based Perovskite Layers for Efficient Solar Cells. *Science* **2017**, *356*, 1376−1379.

(13) Frost, J. M.; Butler, K. T.; Brivio, F.; Hendon, C. H.; van Schilfgaarde, M.; Walsh, A. Atomistic Origins of High-Performance in Hybrid Halide Perovskite Solar Cells. *Nano Lett.* **2014**, *14*, 2584−2590.

(14) Frost, J. M.; Butler, K. T.; Walsh, A. Molecular Ferroelectric Contributions to Anomalous Hysteresis in Hybrid Perovskite Solar Cells. *APL Mater.* **2014**, *2*, 081506.

(15) Liu, S.; Zheng, F.; Koocher, N. Z.; Takenaka, H.; Wang, F.; Rappe, A. M. Ferroelectric Domain Wall Induced Band Gap Reduction and Charge Separation in Organometal Halide Perovskites. *J. Phys. Chem. Lett.* **2015**, *6*, 693−699.

(16) Kutes, Y.; Ye, L.; Zhou, Y.; Pang, S.; Huey, B. D.; Padture, N. P. Direct Observation of Ferroelectric Domains in Solution-Processed $CH_3NH_3PbI_3$ Perovskite Thin Films. *J. Phys. Chem. Lett.* **2014**, *5*, 3335−3339.

(17) Brivio, F.; Frost, J. M.; Skelton, J. M.; Jackson, A. J.; Weber, O. J.; Weller, M. T.; Goñi, A. R.; Leguy, A. M. A.; Barnes, P. R. F.; Walsh, A. Lattice Dynamics and Vibrational Spectra of the Orthorhombic, Tetragonal, and Cubic Phases of Methylammonium Lead Iodide. *Phys. Rev. B: Condens. Matter Mater. Phys.* **2015**, *92*, 144308.

(18) Weller, M. T.; Weber, O. J.; Henry, P. F.; Di Pumpo, A. M.; Hansen, T. C. Complete Structure and Cation Orientation in the Perovskite Photovoltaic Methylammonium Lead Iodide between 100 and 352 K. *Chem. Commun.* **2015**, *51*, 4180−4183.

(19) Brivio, F.; Walker, A. B.; Walsh, A. Structural and Electronic Properties of Hybrid Perovskites for High-Efficiency Thin-Film Photovoltaics from First-Principles. *APL Mater.* **2013**, *1*, 042111.

(20) Hendon, C. H.; Yang, R. X.; Burton, L. A.; Walsh, A. Assessment of Polyanion (BF_4^- and PF_6^-) Substitutions in Hybrid Halide Perovskites. *J. Mater. Chem. A* **2015**, *3*, 9067−9070.

(21) Zong, Y.; Zhou, Y.; Ju, M.; Garces, H. F.; Krause, A. R.; Ji, F.; Cui, G.; Zeng, X. C.; Padture, N. P.; Pang, S. Thin-Film

Transformation of NH_4PbI_3 to $CH_3NH_3PbI_3$ Perovskite: A Methylamine-Induced Conversion-Healing Process. *Angew. Chem., Int. Ed.* **2016**, *55*, 14723−14727.
(22) Eperon, G. E.; Stranks, S. D.; Menelaou, C.; Johnston, M. B.; Herz, L. M.; Snaith, H. J. Formamidinium Lead Trihalide: A Broadly Tunable Perovskite for Efficient Planar Heterojunction Solar Cells. *Energy Environ. Sci.* **2014**, *7*, 982−988.
(23) Stoumpos, C. C.; Frazer, L.; Clark, D. J.; Kim, Y. S.; Rhim, S. H.; Freeman, A. J.; Ketterson, J. B.; Jang, J. I.; Kanatzidis, M. G. Hybrid Germanium Iodide Perovskite Semiconductors: Active Lone Pairs, Structural Distortions, Direct and Indirect Energy Gaps, and Strong Nonlinear Optical Properties. *J. Am. Chem. Soc.* **2015**, *137*, 6804−6819.
(24) De Marco, N.; Zhou, H.; Chen, Q.; Sun, P.; Liu, Z.; Meng, L.; Yao, E.-P.; Liu, Y.; Schiffer, A.; Yang, Y. Guanidinium: A Route to Enhanced Carrier Lifetime and Open-Circuit Voltage in Hybrid Perovskite Solar Cells. *Nano Lett.* **2016**, *16*, 1009−1016.
(25) Savory, C. N.; Walsh, A.; Scanlon, D. O. Can Pb-Free Halide Double Perovskites Support High-Efficiency Solar Cells? *ACS Energy Lett.* **2016**, *1*, 949−955.
(26) Protesescu, L.; Yakunin, S.; Bodnarchuk, M. I.; Krieg, F.; Caputo, R.; Hendon, C. H.; Yang, R. X.; Walsh, A.; Kovalenko, M. V. Nanocrystals of Cesium Lead Halide Perovskites ($CsPbX_3$, X = Cl, Br, and I): Novel Optoelectronic Materials Showing Bright Emission with Wide Color Gamut. *Nano Lett.* **2015**, *15*, 3692−3696.
(27) Kieslich, G.; Sun, S.; Cheetham, A. K. An Extended Tolerance Factor Approach for Organic−inorganic Perovskites. *Chem. Sci.* **2015**, *6*, 3430−3433.
(28) Travis, W.; Glover, E. N. K.; Bronstein, H.; Scanlon, D. O.; Palgrave, R. G. On the Application of the Tolerance Factor to Inorganic and Hybrid Halide Perovskites: A Revised System. *Chem. Sci.* **2016**, *7*, 4548−4556.
(29) Dualeh, A.; Gao, P.; Seok, S. I.; Nazeeruddin, M. K.; Grätzel, M. Thermal Behavior of Methylammonium Lead-Trihalide Perovskite Photovoltaic Light Harvesters. *Chem. Mater.* **2014**, *26*, 6160−6164.
(30) Mosconi, E.; Azpiroz, J. M.; De Angelis, F. *Ab Initio* Molecular Dynamics Simulations of Methylammonium Lead Iodide Perovskite Degradation by Water. *Chem. Mater.* **2015**, *27*, 4885−4892.
(31) Juarez-Perez, E. J.; Hawash, Z.; Raga, S. R.; Ono, L. K.; Qi, Y. Thermal Degradation of $CH_3NH_3PbI_3$ Perovskite into NH_3 and CH_3I Gases Observed by Coupled Thermogravimetry−mass Spectrometry Analysis. *Energy Environ. Sci.* **2016**, *9*, 3406−3410.
(32) Lauer, W. M. Non-Benzenoid Aromatic Compounds. *J. Am. Chem. Soc.* **1960**, *82*, 5259−5260.
(33) Breslow, R.; Groves, J. T.; Ryan, G. Cyclopropenyl Cation. *J. Am. Chem. Soc.* **1967**, *89*, 5048−5048.
(34) Kerber, R. C.; Hsu, C.-M. Substituent Effects on Cyclopropenium Ions. *J. Am. Chem. Soc.* **1973**, *95*, 3239−3245.
(35) Law, D. C.; Tobey, S. W.; West, R. Fluorinated Cyclopropenes and Cyclopropenium Ions. *J. Org. Chem.* **1973**, *38*, 768−773.
(36) Yoshida, Z.-I.; Hirota, S.; Ogoshi, H. Vibrational Spectra of Cyclopropenium Ions. *Spectrochim. Acta* **1974**, *30A*, 1105−1114.
(37) Yoshida, Z.-I.; Ogoshi, H.; Hirota, S. Stability and Ring Deformation Vibration of Cyclopropenium Ions. *Tetrahedron Lett.* **1973**, *14*, 869−872.
(38) Breslow, R.; Groves, J. T. Cyclopropenyl Cation. Synthesis and Characterization. *J. Am. Chem. Soc.* **1970**, *92*, 984−987.
(39) Breslow, R.; Groves, J. T.; Ryan, G. Cyclopropenyl Cation. *J. Am. Chem. Soc.* **1967**, *89*, 5048−5048.
(40) Jacobs, T. L.; Brill, W. F. Haloallenes. *J. Am. Chem. Soc.* **1953**, *75*, 1314−1317.
(41) Kelly, B. D.; Lambert, T. H. Aromatic Cation Activation of Alcohols: Conversion to Alkyl Chlorides Using Dichlorodiphenylcyclopropene. *J. Am. Chem. Soc.* **2009**, *131*, 13930−13931.
(42) Vanos, C. M.; Lambert, T. H. Development of a Catalytic Platform for Nucleophilic Substitution: Cyclopropenone-Catalyzed Chlorodehydration of Alcohols. *Angew. Chem., Int. Ed.* **2011**, *50*, 12222−12226.
(43) Bandar, J. S.; Tanaset, A.; Lambert, T. H. Phase-Transfer and Other Types of Catalysis with Cyclopropenium Ions. *Chem. - Eur. J.* **2015**, *21*, 7365−7368.
(44) Jiang, Y.; Freyer, J. L.; Cotanda, P.; Brucks, S. D.; Killops, K. L.; Bandar, J. S.; Torsitano, C.; Balsara, N. P.; Lambert, T. H.; Campos, L. M. The Evolution of Cyclopropenium Ions into Functional Polyelectrolytes. *Nat. Commun.* **2015**, *6*, 5950.
(45) Binek, A.; Hanusch, F. C.; Docampo, P.; Bein, T. Stabilization of the Trigonal High-Temperature Phase of Formamidinium Lead Iodide. *J. Phys. Chem. Lett.* **2015**, *6*, 1249−1253.
(46) Stoumpos, C. C.; Malliakas, C. D.; Kanatzidis, M. G. Semiconducting Tin and Lead Iodide Perovskites with Organic Cations: Phase Transitions, High Mobilities, and Near-Infrared Photoluminescent Properties. *Inorg. Chem.* **2013**, *52*, 9019−9038.
(47) Quarti, C.; Mosconi, E.; De Angelis, F. Interplay of Orientational Order and Electronic Structure in Methylammonium Lead Iodide: Implications for Solar Cell Operation. *Chem. Mater.* **2014**, *26*, 6557−6569.
(48) Weller, M. T.; Weber, O. J.; Frost, J. M.; Walsh, A. Cubic Perovskite Structure of Black Formamidinium Lead Iodide, α-$[HC(NH_2)_2]PbI_3$, at 298 K. *J. Phys. Chem. Lett.* **2015**, *6*, 3209−3212.
(49) Brivio, F.; Butler, K. T.; Walsh, A.; van Schilfgaarde, M. Relativistic Quasiparticle Self-Consistent Electronic Structure of Hybrid Halide Perovskite Photovoltaic Absorbers. *Phys. Rev. B: Condens. Matter Mater. Phys.* **2014**, *89*, 155204.
(50) Yang, D.; Ming, W.; Shi, H.; Zhang, L.; Du, M.-H. Fast Diffusion of Native Defects and Impurities in Perovskite Solar Cell Material $CH_3NH_3PbI_3$. *Chem. Mater.* **2016**, *28*, 4349−4357.
(51) Fonari, A.; Sutton, C. Effective Mass Calculator. Https://Github.Com/Afonari/Emc, 2012 (accessed Nov 27, 2017).
(52) Togo, A.; Tanaka, I. First Principles Phonon Calculations in Materials Science. *Scr. Mater.* **2015**, *108*, 1−5.

DOI: 10.1021/acs.jpcc.7b11867
J. Phys. Chem. C 2018, 122, 2041−2045